Three-dimensional compatible finite element stress analysis of spinning two-directional FGM annular plates and disks with load and elastic foundation non-uniformities

Abstract

Three-dimensional bending and stress analyses of the rotating two-directional functionally graded annular/circular plates or disks have not been accomplished so far. This task is performed in the present paper, employing a finite element formulation with a C^1-continuity. Therefore, both transversely graded and radially-graded plates may be analyzed as special cases of the present research. Distribution of the transverse loads as well as coefficients of the elastic foundation may be non-uniform. Mixed stress-based and displacement-based edge conditions are considered to cover many practical applications. Compatible Hermitian elements are employed to develop a consistent formulation and avoid jumps in the stress components at the elements interfaces. In contrast to the very limited works presented for the rotating functionally graded circular plates so far, the transverse flexibility and the transverse stress components are also considered in the present research. Finally, influences of the material properties distribution, angular speed, geometric parameters, and the elastic foundation on distributions of the stress and displacement components are investigated for a variety of edge and boundary conditions and some design criteria are extracted.

Keywords

Three-dimensional stress analysis, compatible finite element, two-directional functionally graded materials, rotating annular/circular plates and disks, elastic foundation.

M. Shariyat[*] and R. Mohammadjani

Faculty of Mechanical Engineering, K.N. Toosi University of Technology, Tehran 19991-43344, Iran.

[*] Author email addresses:
m_shariyat@yahoo.com and shariyat@kntu.ac.ir

1 INTRODUCTION

Many engineering components may be modeled as rotating circular plates or disks. Some examples may be found in the power transmission systems, machining devises, circular saws, microwave or baking ovens, photographic facilities, support tables, turbo-machinery, and flywheel and centrifugal

systems. Some of these components (e.g., the clutch or brake disks) may be supported by generally non-uniform elastic foundations that rotate with the assembly. On the other hand, the main advantage of using the functionally graded materials (FGMs) is providing the capability of accurately monitoring changes of the local material properties to optimize the component strength. Therefore, achieving a uniform effective stress to strength ratio in the whole component can be an objective. Depending on the function of the component, it is possible to utilize one-, two- or three-directional distributions of the material properties.

Some researchers used the plate theories for bending analysis of the stationary FG circular plates. Axisymmetric bending and stretching of the functionally graded solid and annular circular plates was studied by Reddy et al. (1999) using the first-order shear deformation plate theory. Ma and Wang (2004) employed the third-order shear deformation plate theory to study axisymmetric bending of the functionally graded circular plates. Golmakani and Kadkhodayan (2011) studied axisymmetric nonlinear bending of an annular functionally graded plate using the finite difference technique.

Due to the contradictory assumptions used in the plate theories, their results may be inaccurate for many applications, especially for the thick plates or disks. Instead, results of the three-dimensional theory of elasticity are exact and more accurate. Assuming the material properties to vary in both transverse and radial directions, Nie and Zhong (2007) investigated axisymmetric bending of the two-directional functionally graded circular and annular plates based on the three-dimensional theory of elasticity using a semi-analytical method. Li et al. (2008a) obtained an elastic solution for axisymmetric bending of FGM circular and annular plates subject to polynomial loads of even order. The problem of a functionally graded, transversely isotropic, magneto–electro-elastic circular plate acted on by a uniform load is treated by Li et al. (2008b) based on the three-dimensional theory of elasticity. Yang et al. (2008) presented an analytical solution for bending of annular plates under uniform loadings. Lei and Zheng (2009) presented an exact solution for axisymmetric bending of functionally graded circular plates under elastically supported and rigid slipping edge conditions. Based on the three-dimensional theory of elasticity, Wang et al. (2010) investigated axisymmetric bending of functionally graded circular plates subjected to Bessel function-type transverse loads using the direct displacement method.

The investigations developed in the field of bending and stress analysis of the rotating circular FG plates or disks in literature are very rare. An analytical solution was developed by Chen and Chen (2007) and Chen et al. (2007) for a rotating transversely-graded axisymmetric annular plate, based on the 2D elasticity equations. No external load was considered. A semi-analytical thermoelasticity solution was presented by Hosseini Kordkheili and Naghdabadi (2007) for axisymmetric hollow and solid rotating disks made of functionally graded materials based on the one-dimensional elasticity, dividing the disk into isotropic annular sub-disks. Using the first-order shear-deformation theory, Bayat et al. (2009a) presented a semi-analytical solution for axisymmetric bending analysis of radially-graded rotating solid and annular disks. Bayat et al. (2009b) extended this work by including the thickness variability and a uniform temperature rise. Axisymmetric thermoelastic analysis of a rotating radially-graded hollow circular disk subjected to radial temperature distribution was performed by Peng and Li (2010) using a one-dimensional elasticity theory.

Reviewing the literature reveals that very limited papers have been published on the two-directional functionally graded circular plates (Nie and Z. Zhong, 2007). Nie and Zhong (2010) investigated dynamic behavior of the two-directional FGM annular plates based on the three-dimensional theory of elasticity using the state-space method combined with the one dimensional differential quadrature method. Recently, some semi-analytical vibration and buckling solutions have been proposed by Alipour et al. (2010), Shariyat and Alipour (2011), and Alipour and Shariyat (2011) for two-directional functionally graded circular plates resting on elastic foundations based on the shear-deformation plate theories and the differential transformation method (DTM).

The above brief review reveals that three-dimensional bending and stress analysis of two-directional functionally graded annular/circular plates resting on elastic foundations has not been performed yet, even for the stationary plates. Some other novelties included in the present research are considering non-uniform distributions of both the transversely imposed load and the elastic coefficient of the foundation. Furthermore, a variety of the mechanical surface and edge conditions is considered. Moreover, the available finite element analyses (even those performed by NASTRAN, ABAQUS, and ANSYS softwares), have been performed based Lagrangian (C^0-continuous) elements. Present results are extracted employing compatible C^1-continuous elements to avoid stress discontinuities at the mutual boundaries of the elements. Effects of the material properties indices, geometric parameters, foundation stiffness, type of the non-uniform distributions of the transverse loads and the stiffness of the elastic foundation, and edge conditions on the bending behavior and stress distribution of the mentioned annular plates/disks are investigated through a parametric study and some design criteria are extracted.

2 THE GOVERNING EQUATIONS

2.1 Description of variations of the material properties

Consider a rotating annular two-directional functionally graded axisymmetric plate with inner radius a, outer radius b, and thickness h resting on an elastic foundation, as shown in Figure 1. In Figure 1, the radial and axial (transverse) coordinates are denoted by r and z, respectively. Generally, both the transversely distributed load and stiffness of the elastic substrate/foundation may vary with the radial coordinate r. The transverse coordinate z of the plate is measured from the bottom surface of the plate and is positive upward. It is assumed that Young's modulus E, Poisson's ratio ν, and the mass density ρ vary in both radial and transverse directions according to exponential functions:

$$E(r,z) = E(0,0)e^{\left(\frac{m_1 z}{h} + \frac{n_1 r}{b}\right)}$$
(1)

$$\rho(r,z) = \rho(0,0)e^{\left(\frac{m_2 z}{h} + \frac{n_2 r}{b}\right)}$$
(2)

$$v(r,z) = v(0,0)e^{\left(\frac{m_3 z}{h} + \frac{n_3 r}{b}\right)}$$
(3)

where $E(0,0)$, $\rho(0,0)$, and $v(0,0)$ are the reference values corresponding to the coordinate origin (of a solid circular plate). m_i and n_i $(i=1,2,3)$ are indices of the material mixture and are assumed to be temperature-independent.
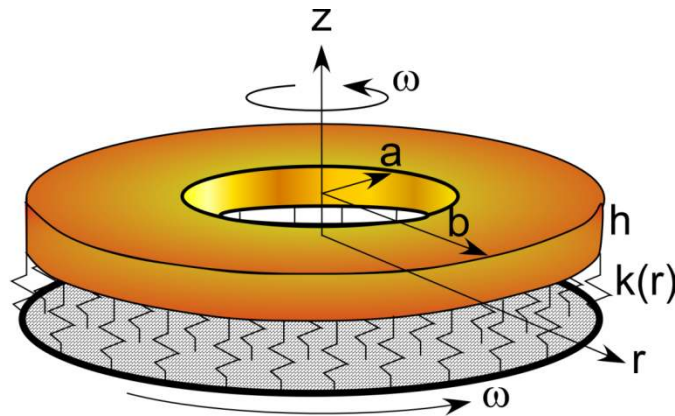

Figure 1   Geometric parameters of a rotating two-directional functionally graded annular plate or disk resting on a non-uniform elastic foundation. The non-uniform transversely distributed loads and the edge conditions are not shown for the sake of clarity.

2.2 The finite element governing equations of the entire plate

Rectangular compatible Hermitian elements are used to discretize the plate. Since the loading and boundary conditions are assumed to be axisymmetric, only the cross section of the plate has to be discretized (Figure 2).
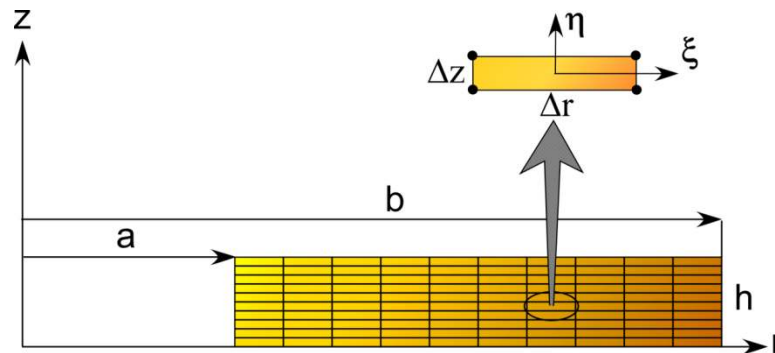

Figure 2   Discretization of the cross section of the plate.

The traditional finite element analysis softwares, e.g., NASTRAN, ANSYS, and ABAQUS, generally use Lagrangian elements with C^0-continuity (Garcia and Proença, 2007, Polat, 2010, Kim and Reddy, 2010). Therefore, the stress components experience jumps at the mutual boundaries of the elements (including the nodal points) (Shariyat and Eslami, 1996, Shariyat, 2009a, Shariyat et al., 2011, Shariyat, 2011a,b,c). For this reason, these softwares use averaging or interpolation techniques among the Gaussian points to cover this shortcoming. In the present research, Hermitian elements are used to avoid this shortcoming. The displacement field within the cross section of the plate may be interpreted based on the Hermitian shape functions as (Reddy, 2006):

$$\delta = \left\{ \begin{array}{c} u \\ w \end{array} \right\} = \left[\begin{array}{cccc} \mathbf{H} & 0 & ... & 0 \\ 0 & \mathbf{H} & ... & 0 \\ ... & ... & ... & ... \\ 0 & 0 & ... & \mathbf{H} \end{array} \right] \Lambda^{(e)} = \mathbf{H}^{(e)} \Lambda^{(e)} \tag{4}$$

where u and w are respectively the radial and transverse displacement components, $\Lambda^{(e)}$ is the vector of the nodal values containing the displacement parameters and their derivatives (Figure 2):

$$\Lambda^{(e)T} = \left\langle\begin{array}{ccccccccc} U_1 & U_{1,\xi} & U_{1,\eta} & U_{1,\xi\eta} & \text{.........} & W_4 & W_{4,\xi} & W_{4,\eta} & W_{4,\xi\eta} \end{array}\right\rangle \tag{5}$$

The natural coordinates $\xi(-1 \leq \xi \leq 1)$ and $\eta(-1 \leq \eta \leq 1)$ are in the radial and transverse directions, respectively and may be related to the global coordinates r and z as follows:

$$r = (m - 1/2 + \xi/2)\Delta r , \quad z = (n - 1/2 + \eta/2)\Delta z \tag{6}$$

where m and n are the element counters in the radial and transverse directions, respectively. Therefore,

$$\frac{\partial}{\partial r} = \frac{\partial}{\partial \xi}\frac{\partial \xi}{\partial r} = \frac{2}{\Delta r}\frac{\partial}{\partial \xi}, \quad \frac{\partial}{\partial z} = \frac{\partial}{\partial \eta}\frac{\partial \eta}{\partial z} = \frac{2}{\Delta z}\frac{\partial}{\partial \eta}$$
$$dr = \frac{\Delta r}{2}d\xi, \quad dz = \frac{\Delta z}{2}d\eta \tag{7}$$

In Eq. (4) [26]:

$$\mathbf{H} = \left\langle \begin{array}{cccc} \mathbf{H}_{11} & \mathbf{H}_{21} & \mathbf{H}_{12} & \mathbf{H}_{22} \end{array} \right\rangle$$
$$\mathbf{H}_{ij} = \left\langle \begin{array}{cccc} H_{0i}^1(\xi)H_{0j}^1(\eta) & H_{1i}^1(\xi)H_{0j}^1(\eta) & H_{0i}^1(\xi)H_{1j}^1(\eta) & H_{1i}^1(\xi)H_{1j}^1(\eta) \end{array} \right\rangle \quad , i = 1,2; j = 1,2 \tag{8}$$

where, each of i and j subscripts is the node number in the ξ and η directions, respectively (1 or 2):

$$H_{01}^1(\xi) = \tfrac{1}{4}\left(1-\xi\right)^2(2+\xi)$$
$$H_{02}^1(\xi) = \tfrac{1}{4}\left(1+\xi\right)^2(2-\xi)$$
$$H_{11}^1(\xi) = \tfrac{1}{4}\left(1-\xi\right)^2(\xi+1)$$
$$H_{12}^1(\xi) = \tfrac{1}{4}\left(1+\xi\right)^2(\xi-1)$$

$$\tag{9}$$

On the other hand, the strain components may be related to the displacement components as:

$$\varepsilon_r = \frac{\partial u}{\partial r} \quad , \quad \varepsilon_\theta = \frac{u}{r} \quad , \quad \varepsilon_z = \frac{\partial w}{\partial z} \quad , \quad \gamma_{rz} = \frac{\partial u}{\partial z} + \frac{\partial w}{\partial r} \tag{10}$$

or in a matrix form:

$$\varepsilon = \mathbf{d}\delta = \mathbf{dH}^{(e)}\Lambda^{(e)} \tag{11}$$

where the superscript "(e)" denotes the element quantity and

$$\varepsilon^T = \left\langle \begin{array}{cccc} \varepsilon_r & \varepsilon_\theta & \varepsilon_z & \gamma_{r\theta} \end{array} \right\rangle, \quad \mathbf{d} = \begin{bmatrix} \dfrac{\partial}{\partial r} & 0 \\[2mm] \dfrac{1}{r} & 0 \\[2mm] 0 & \dfrac{\partial}{\partial z} \\[2mm] \dfrac{\partial}{\partial z} & \dfrac{\partial}{\partial r} \end{bmatrix} \tag{12}$$

So that:

$$\delta\varepsilon^T = \left(\delta\Lambda^{(e)}\right)^T \left(\mathbf{dH}^{(e)}\right)^T \tag{13}$$

According to the generalized Hooke's law, the stress-strain relation may be expressed as:

$$\sigma = \mathbf{d}\varepsilon - \sigma_T \tag{14}$$

where:

$$\sigma^T = \left\langle \begin{array}{cccc} \sigma_r & \sigma_\theta & \sigma_z & \tau_{r\theta} \end{array} \right\rangle,$$

$$\mathbf{d} = \frac{E(r,z)}{\left[1-2v(r,z)\right]\left[1+v(r,z)\right]} \begin{bmatrix} 1-v(r,z) & v(r,z) & v(r,z) & 0 \\ v(r,z) & 1-v(r,z) & v(r,z) & 0 \\ v(r,z) & v(r,z) & 1-v(r,z) & 0 \\ 0 & 0 & 0 & \dfrac{1-2v(r,z)}{2} \end{bmatrix},$$

$$\sigma_T = \frac{E(r,z)\alpha(r,z)}{1-2v(r,z)} \begin{Bmatrix} 1 \\ 1 \\ 1 \\ 0 \end{Bmatrix} \Delta T \tag{15}$$

where σ_r, σ_θ, σ_z, and $\tau_{r\theta}$ are respectively radial, circumferential, axial, and transverse shear stress components, respectively and $\alpha(r,z)$ and ΔT are the thermal expansion coefficient and the temperature rise with respected to the reference temperature, respectively.

The governing equations may be derived using principle of virtual displacements:

$$\delta\Pi = \delta V - \delta W = 0 \tag{16}$$

where V is the strain energy and W is the work of the externally applied loads. For the present analysis, the expanded form of Eq. (16) may be written as:

$$\delta\Pi = \int_\Omega (\delta\varepsilon^T\sigma + \delta\delta^T\mathbf{F})d\Omega + \int_\mathbf{A} k(r)\left(\delta\delta^T\mathbf{R}^T\mathbf{R}\delta\right)_{z=0} d\mathbf{A} - \int_\mathbf{A}\left[\delta\delta^T\mathbf{p}(r)\right]_{z=h} d\mathbf{A} - \int_{\Gamma_i}\left(\delta\delta^T\right)_{r=a}\mathbf{T}_i d\Gamma$$
$$- \int_{\Gamma_o}\left(\delta\delta^T\right)_{r=b}\mathbf{T}_o d\Gamma = 0 \tag{17}$$

It can be easily verified that employing principle of virtual work is equivalent to using Galerkin's technique with the same concept of orthogonality (Shariyat et al., 2010a,b, Shariyat, 2009b, Shariyat, 2012). In Eq. (17), Ω, $\mathbf{A}$, Γ_i, and Γ_o are the volume, in-plane area, inner boundary area, and outer boundary area, respectively. Moreover, Π, $\mathbf{F}$, $\mathbf{p}(r)$, $\mathbf{k}(r)$, and $\mathbf{T}_i$ and $\mathbf{T}_o$ are the total potential energy of the plate, the body force vector that is assumed to be solely due to the plate rotation, the non-uniform traction vector imposed on the upper surface of the plate, the non-uniform stiffness of Winkler's elastic foundation of the plate, and the traction vectors of the inner and outer boundaries (edges) of the plate, respectively

$$\mathbf{F}^T = \left\langle \rho r\omega^2 \quad 0 \right\rangle, \quad \mathbf{p}^T = \left\langle \tau_r \quad p \right\rangle, \quad \mathbf{T}^T = \left\langle \sigma \quad \tau_z \right\rangle \tag{18}$$

ω is the angular speed of the plate and $\mathbf{R}$ is:

$$\mathbf{R} = \left[\begin{array}{cc} \mathbf{0} & \mathbf{I} \end{array} \right] \tag{19}$$

where $\mathbf{I}$ is the identity vector and τ_r and τ_z are the radial and transverse shear tractions of the upper surface and inner or outer boundaries, respectively. Substituting Eqs. (11), (13), and (14) into Eq. (17) leads to the following result:

$$\sum_{e=1}^N \delta\Lambda^{(e)T} \left\{ \int_A \left[\left(d\mathbf{H}^{(e)}\right)^T \left(\mathbf{D}\,d\mathbf{H}^{(e)}\Lambda^{(e)} - \sigma_T\right) + \mathbf{H}^{(e)T}\mathbf{F} \right] rdrdz + \hat{\delta}(z^{(e)} - h)\int_r \mathbf{H}^{(e)}\Big|_{\eta=1} \mathbf{p}(r)r\,dr \right.$$
$$+ \hat{\delta}(z^{(e)})\int_r k(r)\mathbf{H}^{(e)}\Big|_{\eta=-1} \mathbf{R}^T\mathbf{R}\mathbf{H}^{(e)}\Big|_{\eta=-1} \Lambda^{(e)}r\,dr + a\hat{\delta}(r^{(e)} - a)\int_z \mathbf{H}^{(e)}\Big|_{\xi=-1} \mathbf{T}_i\,dz$$
$$\left. + b\hat{\delta}(r^{(e)} - b)\int_z \mathbf{H}^{(e)}\Big|_{\xi=1} \mathbf{T}_o\,dz \right\} = 0 \tag{20}$$

A is the cross section area of the element, N is the number of elements, and $\widehat{\delta}$ is a logical (conditional) term, for example:

$$\widehat{\delta}(z^{(e)} - h) = \begin{cases} 1 & \text{if } h \in z^{(e)} \\ 0 & \text{if } h \notin z^{(e)} \end{cases} \tag{21}$$

Since $\delta \mathbf{\Lambda}^{(e)T}$ is an arbitrary vector, the governing equation of each element will be:

$$\int_{r} \left[\int_{z} \left(\left(\mathbf{dH}^{(e)} \right)^{T} \left(\mathbf{D} \mathbf{dH}^{(e)} \mathbf{\Lambda}^{(e)} - \sigma_{T} \right) + \mathbf{H}^{(e)T} \mathbf{F} \right) dz - \widehat{\delta}(z^{(e)} - h) \mathbf{H}^{(e)} \Big|_{\eta=1} \mathbf{p}(r) \right.$$
$$\left. + \widehat{\delta}(z^{(e)}) k(r) \mathbf{H}^{(e)} \Big|_{\eta=-1} \mathbf{R}^{T} \mathbf{R} \mathbf{H}^{(e)} \Big|_{\eta=-1} \mathbf{\Lambda}^{(e)} \right] r dr - \int_{z} \left[a \widehat{\delta}(r-a) \mathbf{H}^{(e)} \Big|_{\xi=-1} \mathbf{T}_{i} + b \widehat{\delta}(r-b) \mathbf{H}^{(e)} \Big|_{\xi=1} \mathbf{T}_{o} \right] dz = \mathbf{0} \tag{22}$$

or in a compact form:

$$\mathbf{K}^{(e)} \mathbf{\Lambda}^{(e)} = \mathbf{F}^{(e)} \tag{23}$$

where:

$$\mathbf{K}^{(e)} = \int_{a}^{b} \left[\left(\int_{0}^{h} \left(\mathbf{dH}^{(e)} \right)^{T} \mathbf{D} \mathbf{dH}^{(e)} \, dz \right) + \widehat{\delta}(z^{(e)}) k(r) \mathbf{H}^{(e)} \Big|_{\eta=-1} \mathbf{R}^{T} \mathbf{R} \mathbf{H}^{(e)} \Big|_{\eta=-1} \right] r dr$$
$$\mathbf{F}^{(e)} = \int_{a}^{b} \left[\int_{0}^{h} \left(\mathbf{dH}^{(e)} \right)^{T} \left(\sigma_{T} - \mathbf{H}^{(e)T} \mathbf{F} \right) dz + \widehat{\delta}(z^{(e)} - h) \mathbf{H}^{(e)} \Big|_{\eta=1} \mathbf{p}(r) \right] r dr \tag{24}$$
$$+ \int_{0}^{h} \left[a \widehat{\delta}(r-a) \mathbf{H}^{(e)} \Big|_{\xi=-1} \mathbf{T}_{i} + b \widehat{\delta}(r-b) \mathbf{H}^{(e)} \Big|_{\xi=1} \mathbf{T}_{o} \right] dz$$

The governing equation of the entire plate may be established by assembling the element matrices [Eq. (24)]:

$$\mathbf{K} \widehat{\mathbf{\Lambda}} = \widehat{\mathbf{F}} \tag{25}$$

where $\widehat{\mathbf{\Lambda}}$ is the nodal quantities vector of the whole plate.

When calculating the integrals appeared in Eq. (24), the differential quantities of the global coordinate have to be substituted from Eq. (7). Therefore, the resulting integrals may be calculated numerically, using the Gauss-Legendre method [31].

3 BOUNDARY CONDITIONS

In each row of the system of equations (25), either the nodal quantity or the right-hand side expression has to be known. Since the traction-type boundary conditions are included implicitly in Eq. (24), only the displacement-based or the stress resultant edge conditions have to be imposed

The traditional edge conditions that are commonly used for the plate theories cannot lead to accurate results in the elasticity analyses. Some of the edge and regularity conditions that are considered in the present research for the circular (solid) plate are:

a) Clamped edge.

b) Simply-supported edge.

Denoting the clamped, simply-supported, and free edges respectively by C, S, and F symbols, some of the considered edge conditions of the annular plates may be introduced as:

a) C-F edge condition.

b) C-C edge condition.

c) C-S edge condition.

d) F-F edge condition.

e) S-C edge condition.

f) S-S edge condition.

g) F-C edge condition.

h) S-F edge condition.

i) F-S edge condition.

While the C and F type boundary conditions can be imposed directly, the simply-supported boundary condition requires that resultant of the radial stresses, i.e., the moment per unit length M_r, to be equal to zero:

$$
\begin{aligned}
M_r &= \int_0^h \sigma_r z dz = \int_0^h \mathbf{D} \left\langle \begin{array}{cccc} 1 & 0 & 0 & 0 \end{array} \right\rangle (\varepsilon - \sigma_\mathbf{T}) z \, dz \\
&= \frac{\Delta z^2}{2} \sum_s \int_{-1}^1 \mathbf{D} \left\langle \begin{array}{cccc} 1 & 0 & 0 & 0 \end{array} \right\rangle (\mathbf{dH}^{(s)} \Lambda^{(s)} - \sigma_\mathbf{T}) (n - 1/2 + \eta/2) d\eta
\end{aligned}
\tag{26}
$$

where s is the element counter in the transverse direction (for elements located at the mentioned edge). For a circular/annular plate with a specified edge moment (M_0), the edge condition $M_r = M_0$ may be used instead.

Boundary conditions may be incorporated in the system of equations appeared in Eq. (24) either by means of the penalty method (Shariyat, 2010a,b) or by substituting one arbitrary row corresponding to the relevant element(s) by the mentioned condition.

4 RESULTS AND CONCLUSIONS

Example 1: To verify results of the present research for the rotating circular/annular plates, an isotropic solid circular plate previously analyzed by Chen et al. (2007) is reconsidered. Simultaneous effects of the rotation and material heterogeneity will be investigated in the next examples. The elastic coefficients used by Chen et al. (2007), correspond to a general anisotropic case and cannot be used for the FGM plates. Similar to Chen et al. (2007), neither external loads nor edge conditions are imposed on the plate (the edge is free). The plate information is:

$$
a = 0, \quad b = 1m, \quad h = 0.1m, \quad E = 286 \frac{(1+v)(1-2v)}{(1-v)} GPa, \quad \rho = 7600 \frac{kg}{m^3}, \quad v = 0.385, \quad P(r), k(r) = 0, \quad \omega = 62.8 \frac{rad}{s}
$$

The following dimensionless parameters are defined to extract the results:

$$\Sigma_i = \frac{\sigma_i}{\rho\omega^2 b^2} \quad , \quad U = \frac{u c_{11}^0}{\rho\omega^2 b^3} \quad , \quad W = \frac{w c_{11}^0}{\rho\omega^2 b^3} \qquad (c_{11}^0 = 286 GPa)$$

Variations of the displacement as well as the stress components of the bottom surface ($z=0$) are illustrated in Figures 3 and 4, respectively and compared with results of Chen et al. (2007). As it may readily be deduced, there is a good agreement between the results.

(a)

(b)
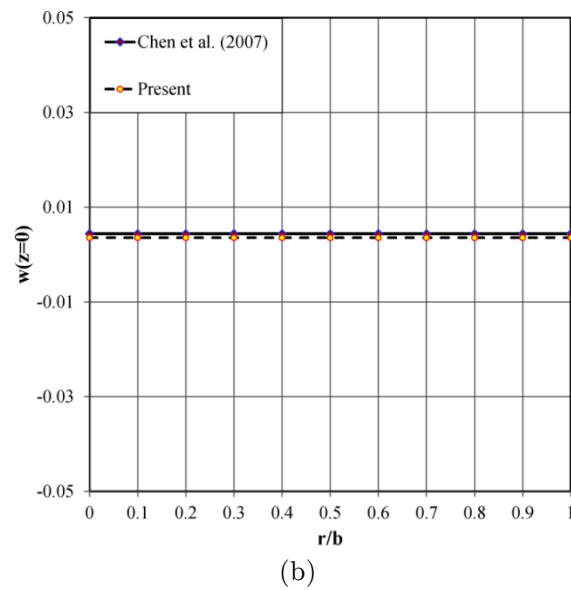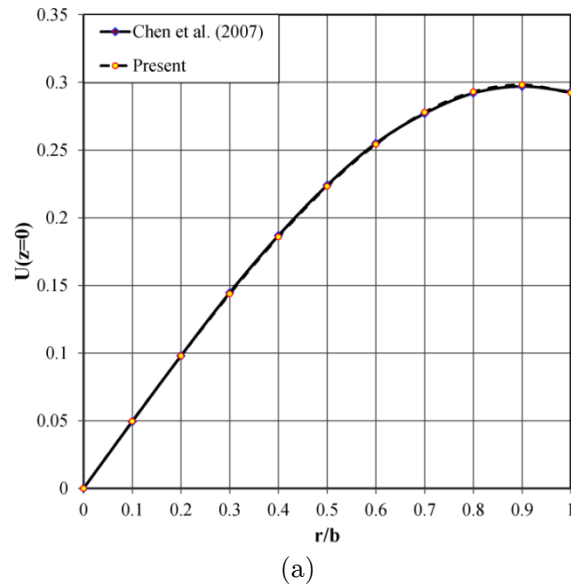
Figure 3   Radial variations of the displacement components of the bottom surface of the rotating isotropic plate.
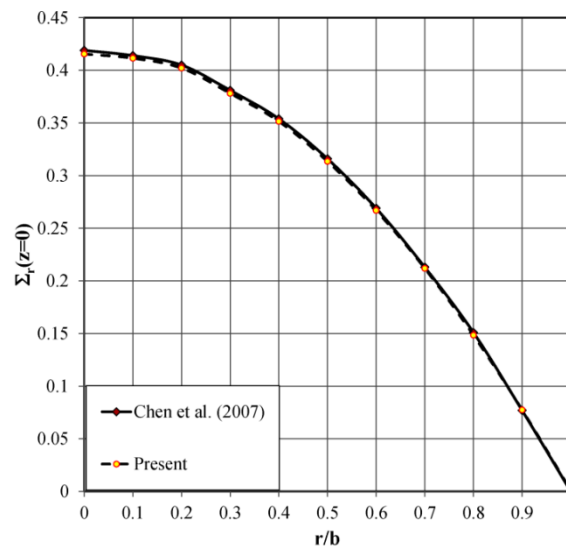
(a)
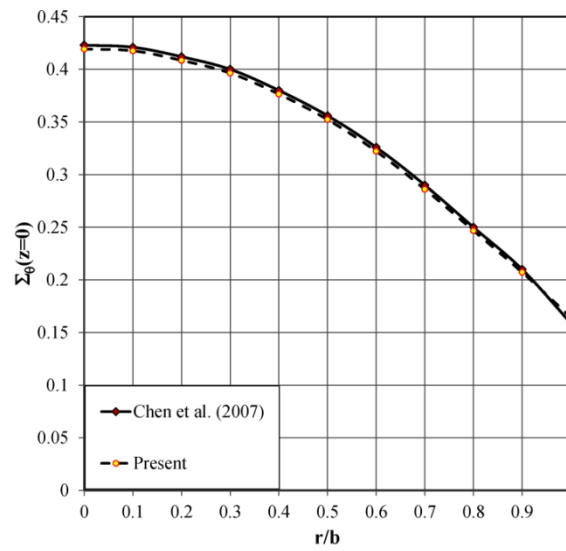
(b)

Figure 4   Radial variations of the in-plane stress components of the bottom surface of the rotating isotropic plate.

Example 2: To evaluate the accuracy of the present three-dimensional elasticity approach, an example is adopted from a work by Sburlati and Bardella (2011). Sburlati and Bardella (2011) proposed an analytical solution for stationary solid transversely-graded clamped circular plates under certain transverse pressures. In this regard, the following data are used:

$$a = 0, \ b = 45mm, \ h = 15mm, \ E_0 \equiv E(0,0) = 45 \ MPa, \ E_h \equiv E(0,h) = 4500 \ MPa, \ m_1 = -2k_1h = 4.605,$$
$$n_1 = 0, \ \omega, \ k(r) = 0, \ P(r) = J_0(\varphi_1 r) \ MPa$$

where $\varphi_1 = z_1^0 / b$ and z_1^0 is the first positive root of $J_0(x)$, the zero-order Bessel function and is equal to 2.404826. The imposed transverse pressure may be expressed with a good accuracy as:

$$P(r) = 1 - \frac{(\varphi_1 r)^2}{4} + \frac{(\varphi_1 r)^4}{64} - \frac{(\varphi_1 r)^6}{2304} + \frac{(\varphi_1 r)^8}{147456} \quad MPa$$

Three sets of the Poisson ratio are considered:

(1) $v = 0.3$

(2) $v = 0.499$

(3) $v_0 \equiv v(0,0) = 0.499$, $v_h \equiv v(0,h) = 0.01$ ($m_3 = -2k_v h = -3.91$, $n_3 = 0$) where

$$k_1 = \frac{1}{2h} ln\left(\frac{E_0}{E_h}\right) \cong -0.1535 \ mm^{-1} \quad , \quad k_v = \frac{1}{2h} ln\left(\frac{v_0}{v_h}\right) \cong 0.1303 \ mm^{-1}$$

In Sburlati and Bardella (2011) paper, the coordinate z is measured from the top surface of the plate and is downward positive. Various combinations of the stress distributions are determined and compared with those of Sburlati and Bardella (2011) paper. In the first stage, the through-the-thickness distributions of the radial and transverse shear stresses of various radial sections are plotted in Figures 5 and 6, respectively for case (1). As Figure 5 shows, due to the bending-extension coupling caused by the non-homogeneous material properties and Poisson's effect caused by the transverse loads, the upper layer of the plate tends to expand. For this reason, the radial stresses of this layer are negative in the neighborhood of the center section of the plate whereas they are positive in the neighborhood of the edge of the plate. This fact justifies the discrepancy appeared in the through-the-thickness distribution of the radial stress at $r=b$. On the other hand, since the neutral surface shifts toward regions with higher elasticity moduli, the maximum transverse shear occurs in the neighborhood of this layer. For this reason, the maximum values of the transverse shear stress have occurred at a fixed location above the mid-surface of the plate (at $z/h \cong 0.2$). This fact is independent of the location of the section or the transverse loading pattern (as in the homogeneous plates or beams). Based on these facts, it seems that present results are slightly more accurate than those of Sburlati and Bardella (2011) paper.

In the next stage, the through-the-thickness distributions of the transverse displacement component and the radial stress are plotted for the center section of the plate and are shown in Figures 7 and 8, respectively, for the three mentioned Poisson ratio distributions, and compared with results of Sburlati and Bardella (2011). Generally, present results are in excellent agreement with results of Sburlati and Bardella (2011).
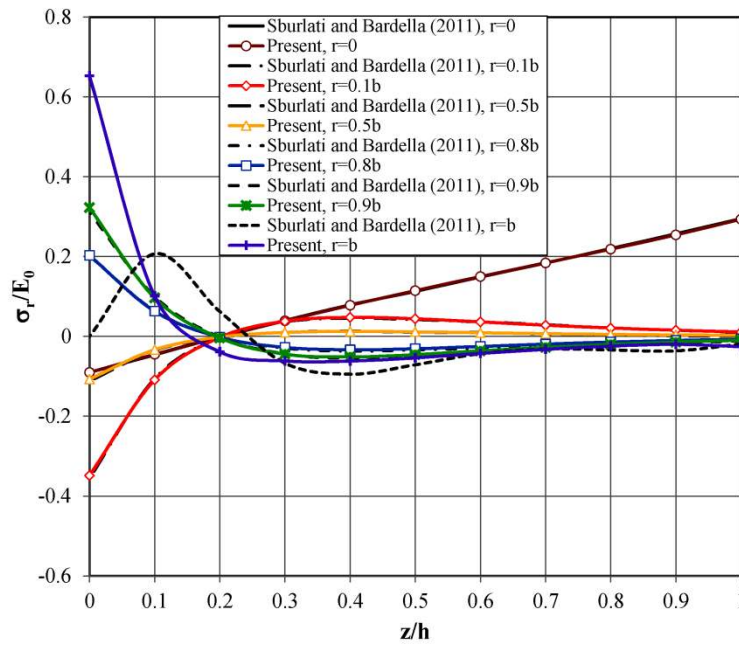
Figure 5   A comparison among the through-the-thickness radial stress distributions, at various radial sections.
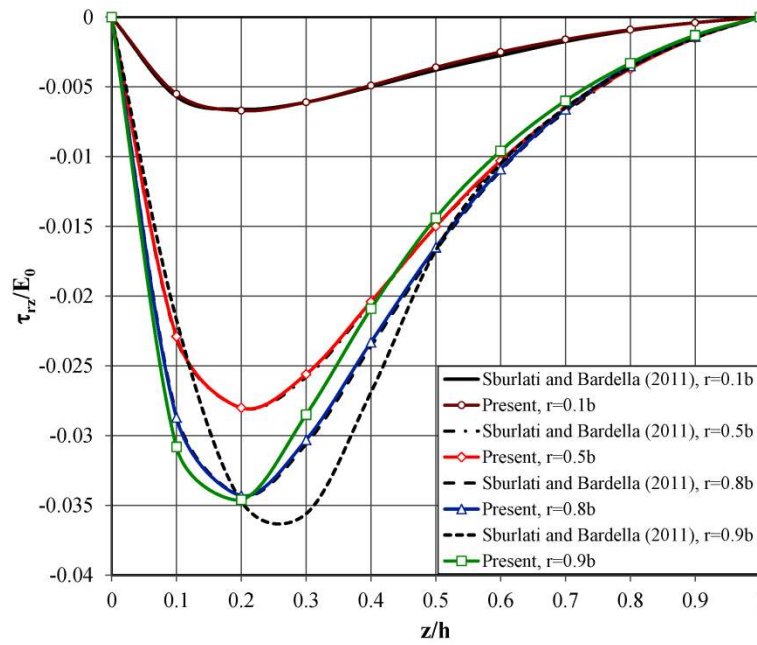

Figure 6   A comparison among the through-the-thickness transverse shear stress distributions, at various radial sections.
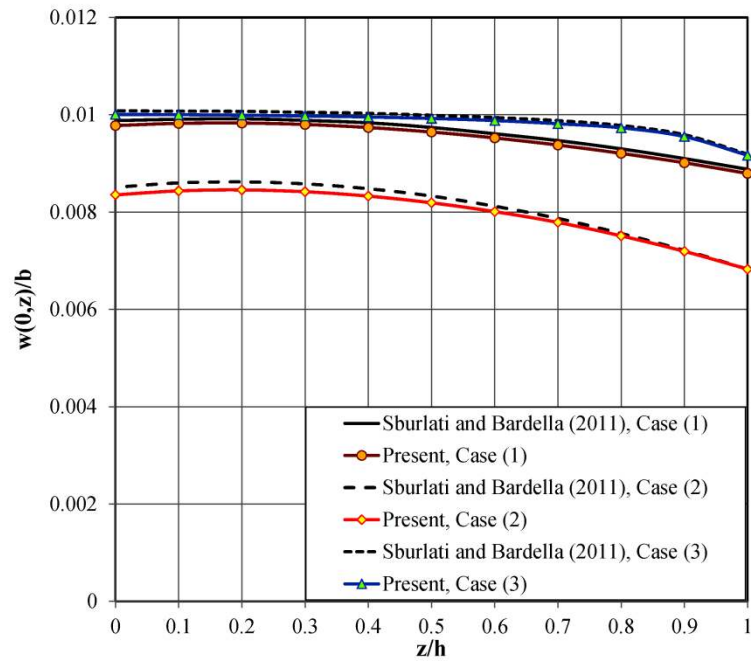
Figure 7   A comparison among the-through-the thickness distributions of the transverse displacement component of the center section of the plate, for various Poisson's ratio distributions.
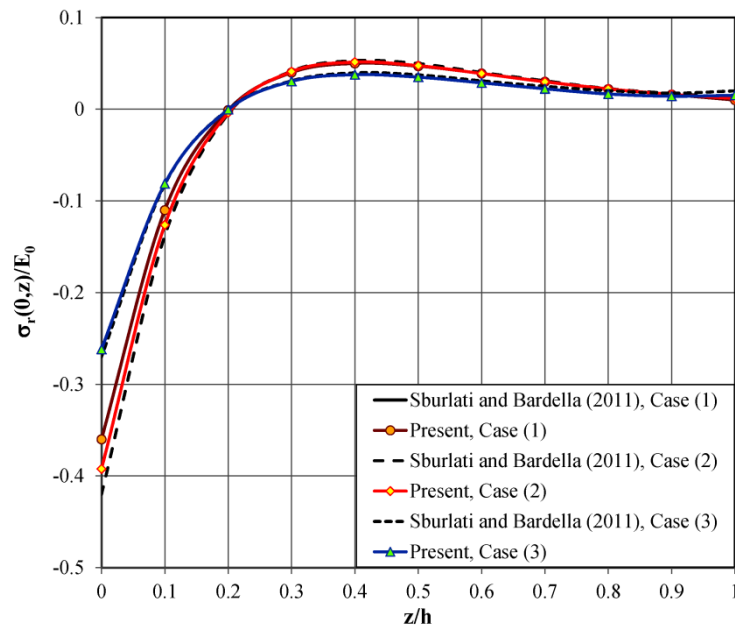

Figure 8   A comparison among the-through-the thickness distributions of the radial stress of the center section of the plate, for various Poisson's ratio distributions.

Example 3:   As a starting point for presenting new results, deformation patterns of a clamped-clamped two-directional functionally graded annular plate with the following information are studied:

$a = 100mm, \quad b = 500mm, \quad h = 50mm, \quad E_0 = 286GPa, \quad v = 0.25, \quad m_1 = 0.5 \quad, \quad n_1 = 1$

Results are plotted for $P(r) = 12.5, 25, 50, 100, 200 \, MPa$, for a better visualization in Figures 9 to 15. Figures 9 and 10 present plots for the dimensionless in-plane (u/P) and transverse (w/P) displacement components, respectively. Based on the chosen geometric parameters, the plate is relatively thick and thus, effects of both the transverse pressure and the edge moments are equally significant. As Figures 9, 11, and 12 show, signs of the in-plane displacement components of the upper and lower layers are opposite and their magnitudes are not similar (as Figures 13 and 14 confirm). On the other hand, due to the material heterogeneity (and consequently, variations of location of the neutral surface in the interval $0.5 < z/h < 0.6$ as one proceeds in the radial direction), there is a bending-extension coupling. It is known that the resulting stresses and displacements due to edge bending are identical to that of a thick cylinder subjected to external and internal pressures [35]. Although the material properties vary exponentially in the transverse direction, since the stress distribution is a result of an equilibrium rather than a kinematic requirement, the trough-the-thickness distribution of the radial displacement component (as the radial stress component that is not shown) is somewhat linear and attains its maximum at layers whose moduli of elasticity are minimum.

Figure 16 shows effects of various edge conditions (CC, CS, SC, and SS) on the dimensionless lateral deflection of the bottom surface of the annular plate. As it may be expected, plates whose edges have more movability, experience greater deflections. So that, the maximum and minimum lateral deflections belong to the SS and CC edge conditions, respectively.
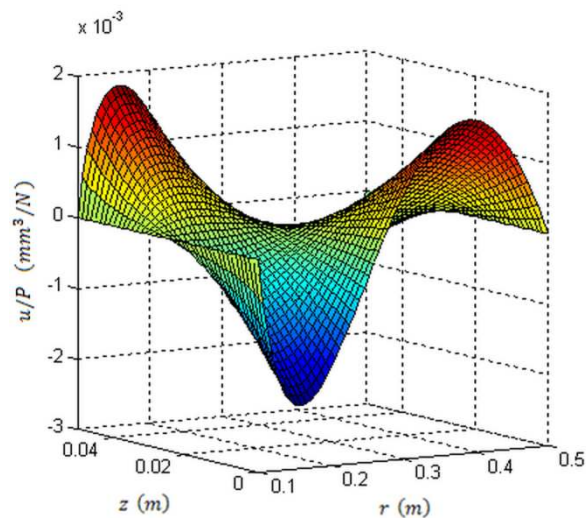

Figure 9   Three-dimensional representation of the simultaneous radial and through-the-thickness variations of the in-plane displacement component of the clamped-clamped two-directional functionally graded annular plate.
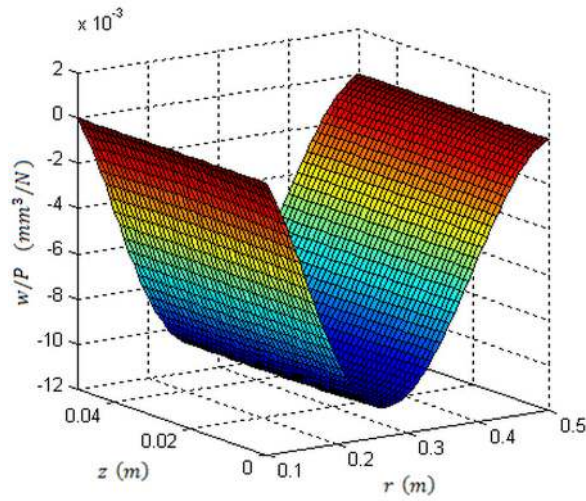
Figure 10   Three-dimensional representation of the simultaneous radial and through-the-thickness variations of the transverse displacement component of the clamped-clamped two-directional functionally graded annular plate.
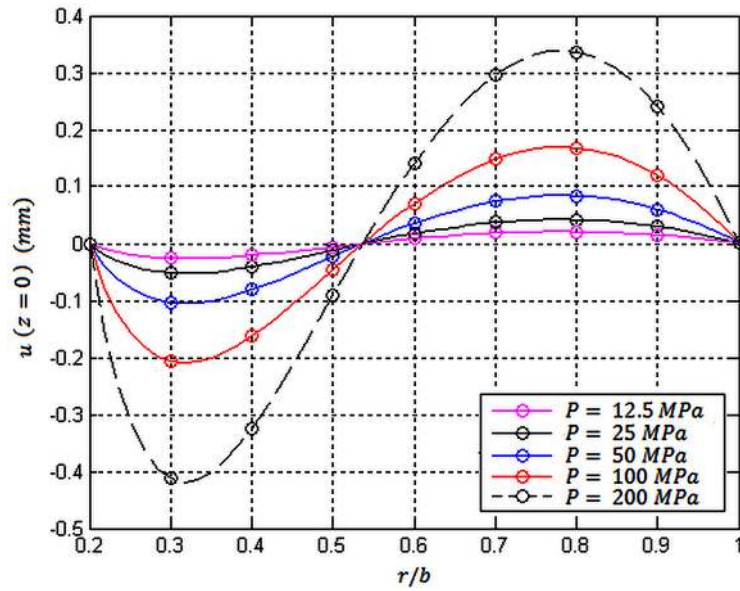

Figure 11   Radial variations of the in-plane displacement component of the bottom surface of the clamped-clamped two-directional functionally graded annular plate.
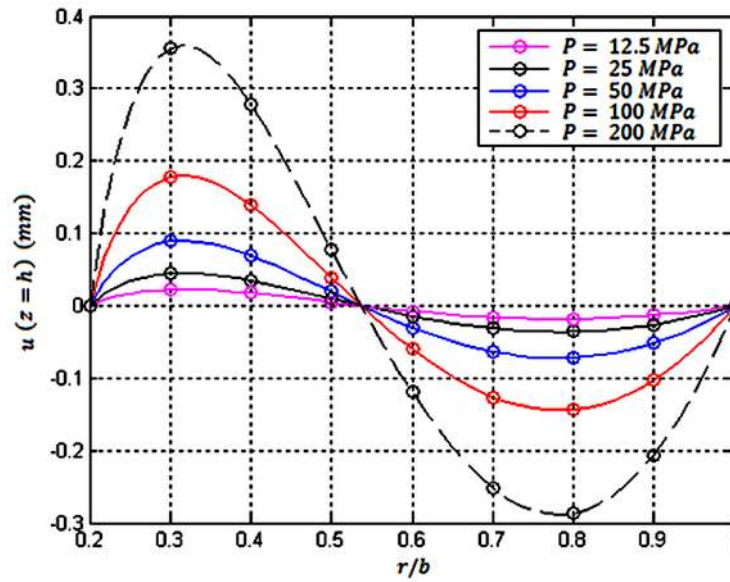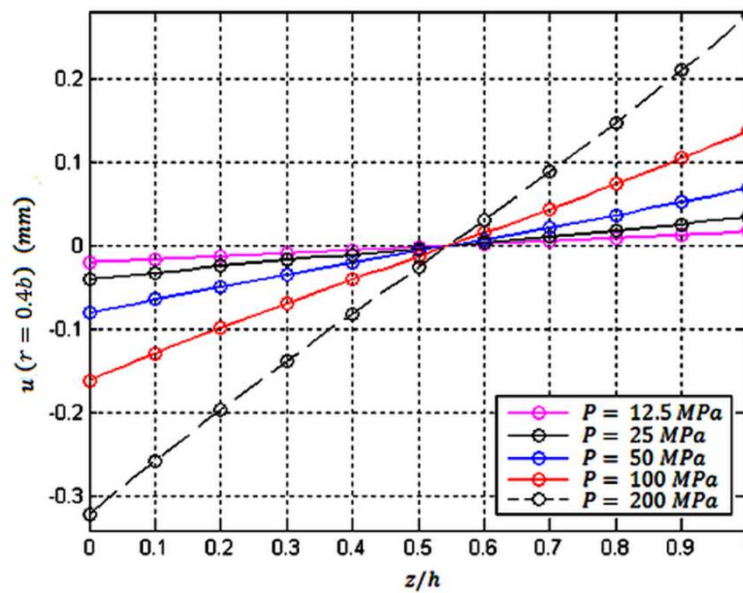
Figure 12   Radial variations of the in-plane displacement component of the upper surface of the clamped-clamped two-directional functionally graded annular plate.

Figure 13   Through-the-thickness variations of the in-plane displacement component of the clamped-clamped two-directional functionally graded annular plate, at $r=0.4b$.
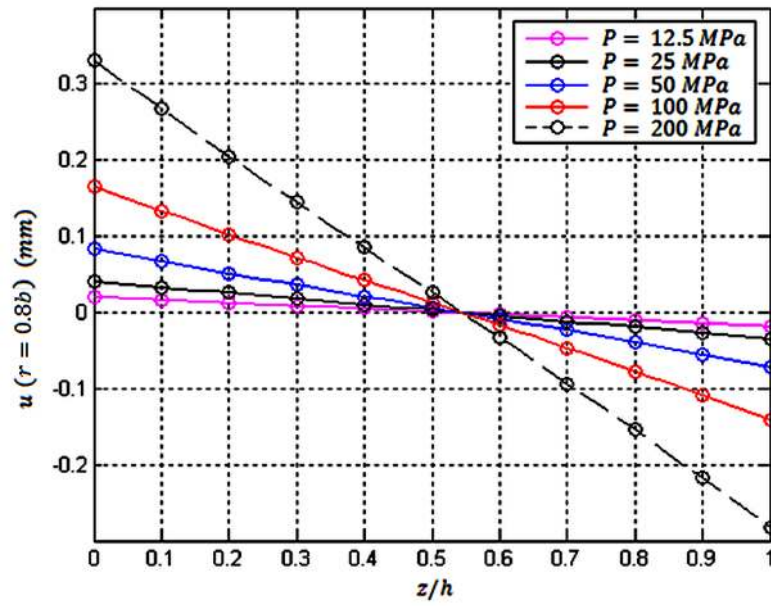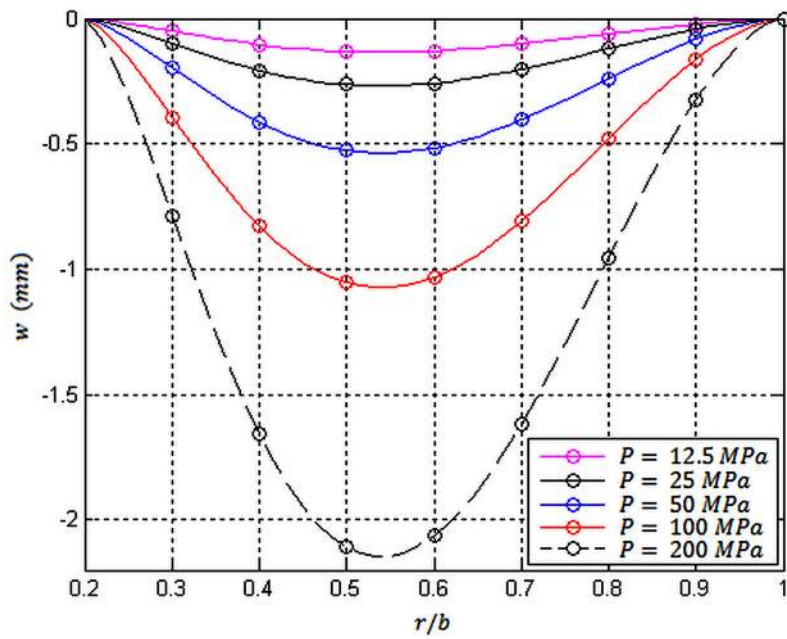
Figure 14   Through-the-thickness variations of the in-plane displacement component of the clamped-clamped two-directional functionally graded annular plate, at *r=0.8b*.

Figure 15   Radial variations of the transverse displacement component of the bottom surface of the clamped-clamped two-directional functionally graded annular plate.
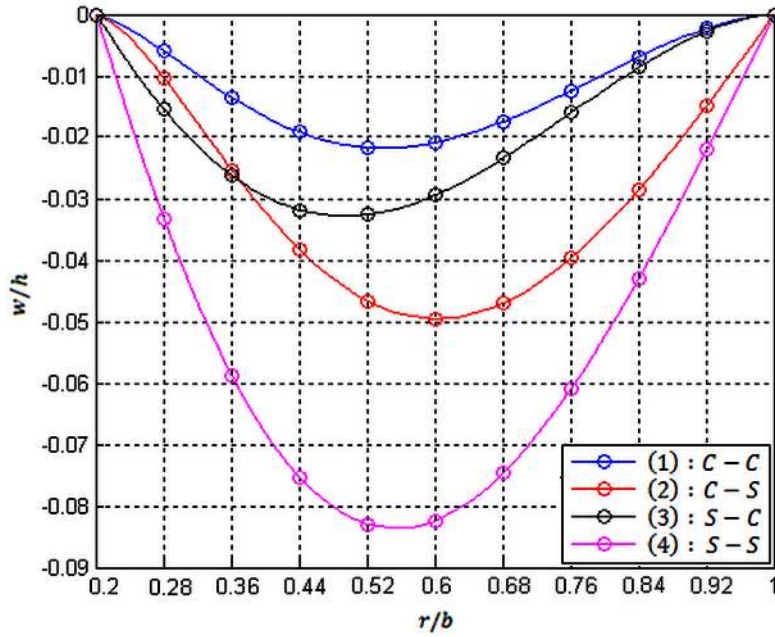
Figure 16   Influence of the edge conditions on the dimensionless lateral deflection of the bottom surface of the two-directional functionally graded annular plate.

Example 4: A stress analysis is performed in the present example for a clamped-clamped two-directional functionally graded annular plate subjected to a uniformly distributed transverse load, resting on an elastic foundation. The following dimensionless parameters are defined to extract the results:

$$R = \frac{r}{a}, \quad U = \frac{u}{h}, \quad W = \frac{w}{h}, \quad k^* = \frac{k\,h}{C_{33}^0} \qquad \left(C_{33}^0 = \frac{\left[1 - \nu(r,z)\right]E(r,z)}{\left[1 - 2\nu(r,z)\right]\left[1 + \nu(r,z)\right]} \right)$$

Results are calculated based on the following data:

$$a = 100\,mm, \quad b = 150\,mm, \quad h = 40\,mm, \quad E = 151\,GPa, \quad \upsilon = 0.3, \quad m_1 = n_1 = 1, \quad P = 1\,GPa, \quad k^* = 1$$

The through-the-thickness distributions of the dimensionless displacement components, the in-plane stress components, and the transverse normal and shear stresses of the mid-section of the plate ($R=0.575$) are depicted in Figures 17, 18, and 19, respectively.

Based on results illustrated in Figures 18 and 19, in the present example:

$$\left|\sigma_z\right| > \left|\sigma_\theta\right|, \left|\sigma_r\right| > \left|\tau_{rz}\right|$$

while in the global plate theories (equivalent single layer theories; e.g., the third-order shear deformation theory), it is assumed that

$$\left|\sigma_\theta\right|, \left|\sigma_r\right| \gg \left|\tau_{rz}\right| \gg \left|\sigma_z\right|$$

In other words, results of the plate theories may be inaccurate for plates resting on elastic foundations. Furthermore, due to the same fact, in these cases, the transverse flexibility of the plate cannot be ignored, as it may be inferred from Figure 17. Moreover, order of the transverse displacement component is much higher than the in-plane one.
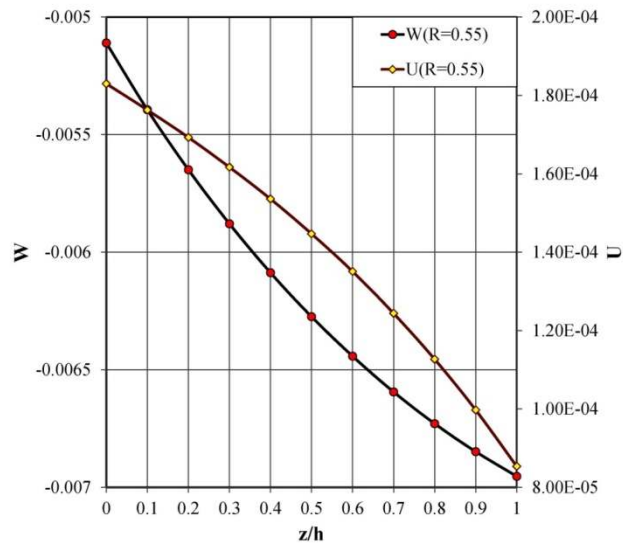

Figure 17   The through-the-thickness distributions of the displacement components of the mid-section of a transversely loaded two-directional functionally graded clamped annular plate resting on an elastic foundation.

A quick glance at Figure 18 reveals that the in-plane stress field may be considered to be a result of a superposition of a hydrostatic pressure field $(\sigma_\theta = \sigma_r)$ and a bending stress field. Based on Figure 19, the maximum shear stress occurs around the neutral plate and below the mid-plane.
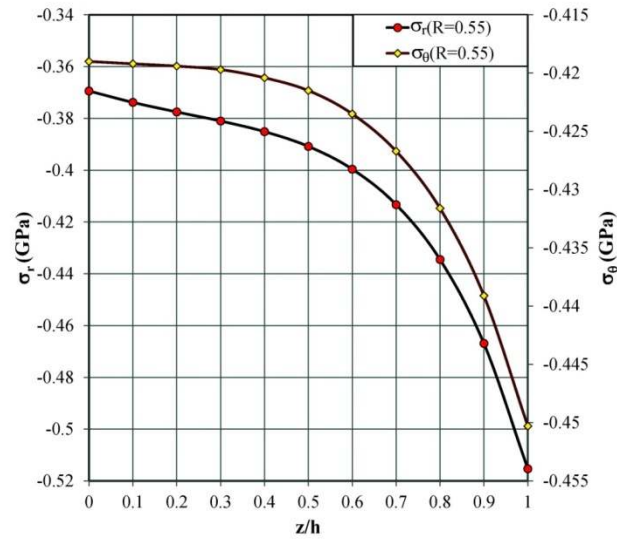
Figure 18   The through-the-thickness distributions of the in-plane stress components of the mid-section of a transversely loaded two-directional functionally graded clamped annular plate resting on an elastic foundation.
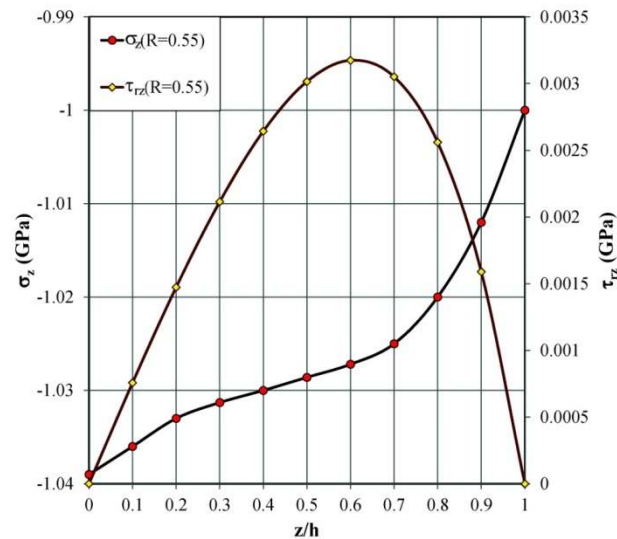

Figure 19   The through-the-thickness distributions of the transverse stress components of the mid-section of a transversely loaded two-directional functionally graded clamped annular plate resting on an elastic foundation.

Example 5: Finally, a comprehensive sensitivity analysis is performed for a clamped-clamped functionally graded annular plate with the following information:

$$a = 100mm, \quad b = 500mm, \quad h = 50mm, \quad E_0 = 180GPa, \quad v = 0.3$$

The following analyses are made to perform the mentioned sensitivity analysis:

(i) In the first stage, a stationary annular plate with $P(r) = 200\,MPa$ is analyzed for the following distinct cases:

Case (A) : A radially − graded plate $(m_i = 0)$ with the following sub − cases:

(1) $n_i = -2$,

(2) $n_i = -1$,

(3) $n_i = 0$,

(4) $n_i = 1$,

(5) $n_i = 2$,

Case (B) : A radially − graded plate $(n_i = 0)$ with the following sub − cases:

(1) $m_i = -2$,

(2) $m_i = -1$,

(3) $m_i = 0$,

(4) $m_i = 1$,

(5) $m_i = 2$.

where i takes the values 1 or 2.

(ii) A two-directional functionally graded $(m_1 = n_1 = 1)$ annular plate with the following uniform and non-uniform loads:

(1) $P(r) = 200\,MPa$,

(2) $P(r) = 1000\,r - 100\ \ MPa$,

(3) $P(r) = -1000\,r + 500\ \ \ MPa$.

(iii) A two-directional functionally graded $(m_1 = n_1 = 1)$ annular plate with a uniform $P(r) = 200\,MPa$ load and one of the following coefficients of the elastic foundation:

(1) $k_1 = 0$,

(2) $k_1 = 0.001$,

(3) $k_1 = 0.01$.

where :

$k_1 = kh / E_0$

(iv) A two-directional functionally graded $(m_1 = n_1 = 1)$ annular plate with a uniform $P(r) = 200\ MPa$ load and one of the following angular speeds:

(1) $\omega = 0$,

(2) $\omega = 20000\,RPM$.

Although variations of all the displacement and stress components may be plotted, only results that lead to more adequate conclusions are reported here to save space.

The radial distributions of the dimensionless lateral deflection of the bottom surface and the through-the-thickness distributions of the radial stress of the inner boundary (the maximum stresses, occur at that boundary) of case (A) of analysis (i) are illustrated respectively in Figures 20 and 21 and some results for case (B) are plotted in Figures 22 and 23. Results shown in Figure

20 confirm that for a specified m_i value, bending/extensional rigidity of the cross sections increases as higher n_i values are adopted. For this reason, the maximum lateral deflection has occurred before the mid-section $r/b = 0.6$ for negative n_i values and after that section for positive n_i values. From Figure 21, it may be concluded that generally, although the through-the-thickness distribution of the radial stress of the thick plate may not be a linear one, the deviations from the linear distribution are ignorable for the middle layers. It is evident that in addition to the bending of the plate, the exerted transverse load causes the layers to expand, especially in layers that are adjacent to the top or bottom (when an elastic foundation exists) layer. Figure 22 reveals that although the lateral deflection of the plate may decrease for greater m_i values, location of the maximum lateral deflection is almost independent of m_i. As discussed in the foregoing example, in this case, the dominant in-plane stress field is the hydrostatic one. For this reason, radial distribution of the hoop stress of the mid-surface is investigated in Figure 23 to provide results diversity.

Analysis (ii) has been adopted to show that location of the maximum lateral deflection is dependent on both the radial material index and the load distribution. Therefore, by choosing a proper material gradient, location of the maximum deflection can be shifted. For a uniform load distribution, location of the maximum lateral deflection occurrence is mainly affected by the radial material index (Figure 24). However, non-uniform load distribution may affect this location. The relevant through-the-thickness distributions of the radial stress of the mid-section of the two-directionally graded annular plate are plotted in Figure (25).

In the previous examples, it has been proven that increasing the foundation stiffness reduces both the displacement components and the in-plane stress components. Figure (26) that illustrates influence of the foundation stiffness on the dimensionless lateral deflection of the bottom surface of the two-directional functionally graded plate, confirms the first fact. However, as Figure (27) demonstrates, the transverse normal stress component increases with the foundation stiffness.

Effects of the angular speed on the dimensionless radial displacement component of the top surface and radial stress of the mid-surface of a transversely loaded two-directional functionally graded annular plate [analysis (iv)] are illustrated in Figures (28) and (29), respectively. As it may be deduced from Figure (28), due to the resulting radial body force and the bending-extension coupling, the initial compression in the top layer of the plate in the neighborhood of the outer edge due to imposing the transverse load and the bending moment has been changed to extension. In the other words, the extension caused by the centrifugal forces had a significant influence. The material shifting due to the mentioned centrifugal forces, superimposes extensional and compressive radial stresses on the initial radial stress distribution of the inner and outer regions of the plate, respectively (Figure 29).
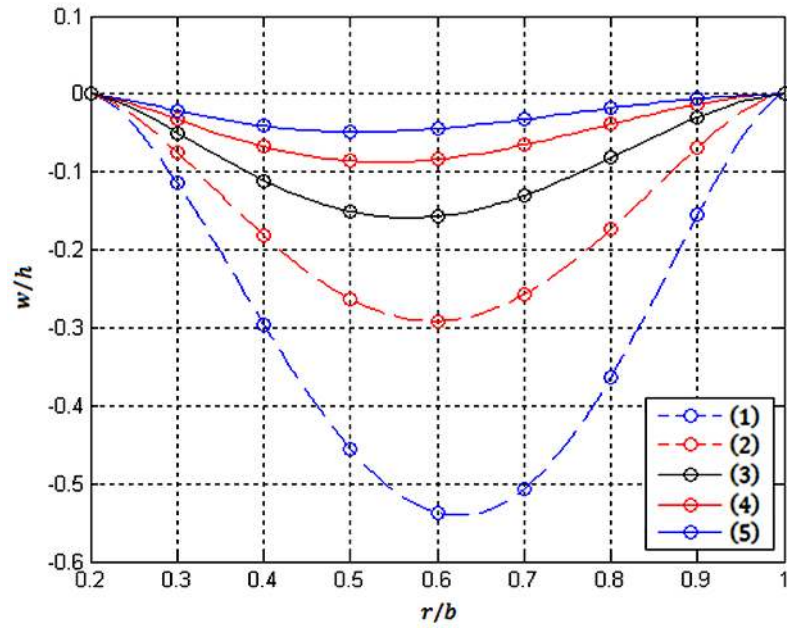
Figure 20 Radial variations of the dimensionless lateral deflection of the bottom surface of the radially-graded clamped-clamped annular plate, for various material indices [Case (A) of analysis (i)].
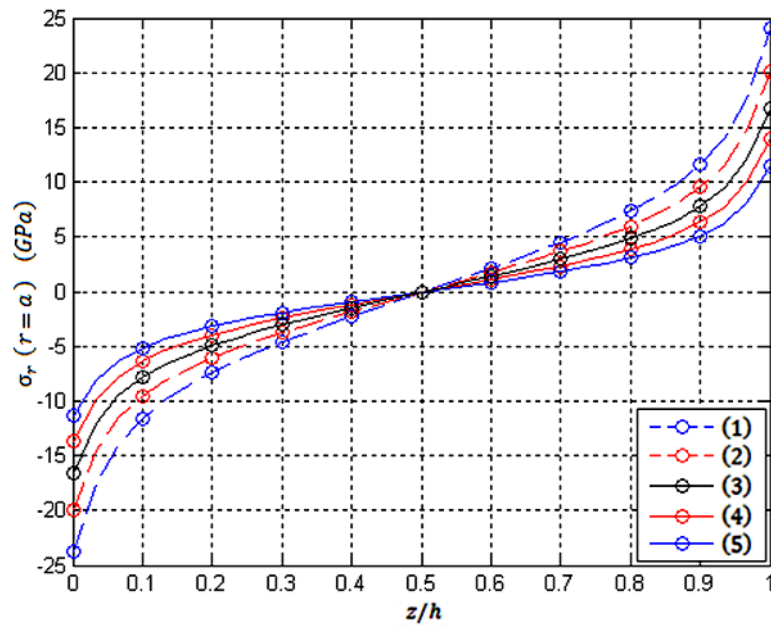

Figure 21 Through-the-thickness distribution of the radial stress of the radially-graded clamped-clamped annular plate, for various material indices [Case (A) of analysis (i)].
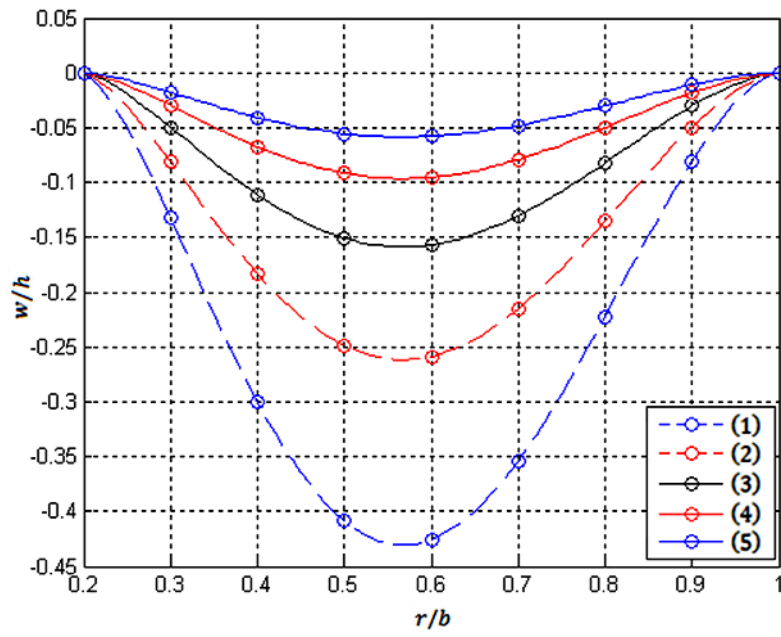
Figure 22   Radial variations of the dimensionless lateral deflection of the bottom surface of the transversely-graded clamped-clamped annular plate, for various material indices [Case (B) of analysis (i)].
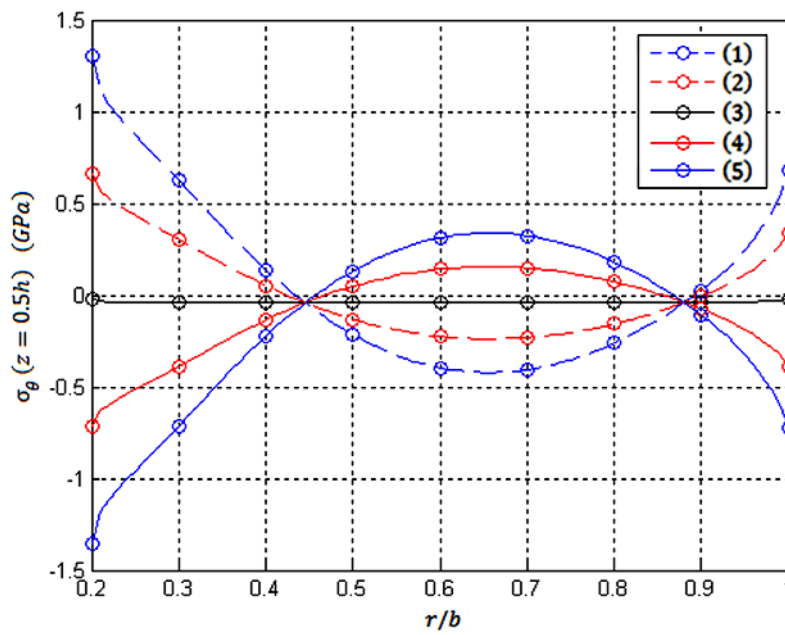

Figure 23   Radial variations of the hoop stress of the mid-surface of the transversely-graded clamped-clamped annular plate, for various material indices [Case (B) of analysis (i)].
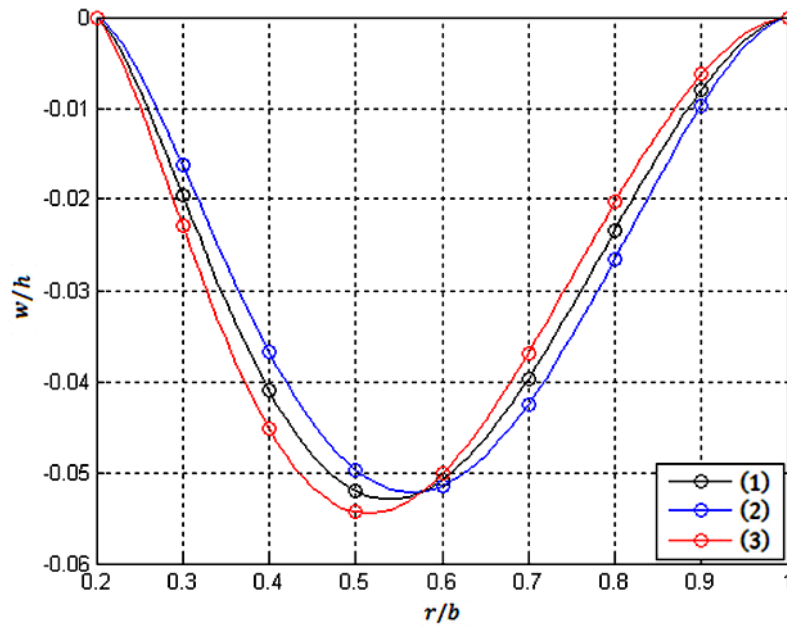
Figure 24   Radial variations of the dimensionless lateral deflection of the bottom surface of the two-directionally graded clamped-clamped annular plate, for various load distributions of analysis (ii).
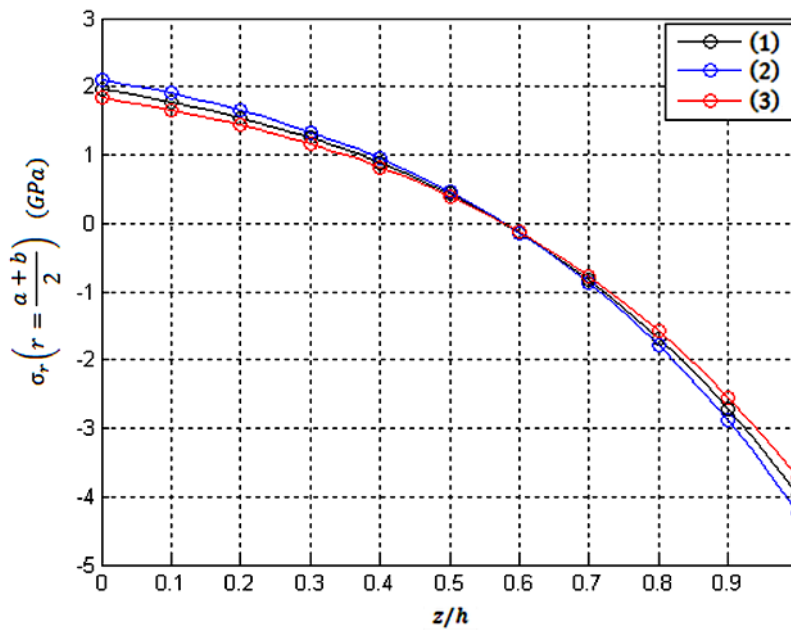

Figure 25   The through-the-thickness distribution of the radial stress of the mid-section of the plate, for various load distributions [analysis (ii)].
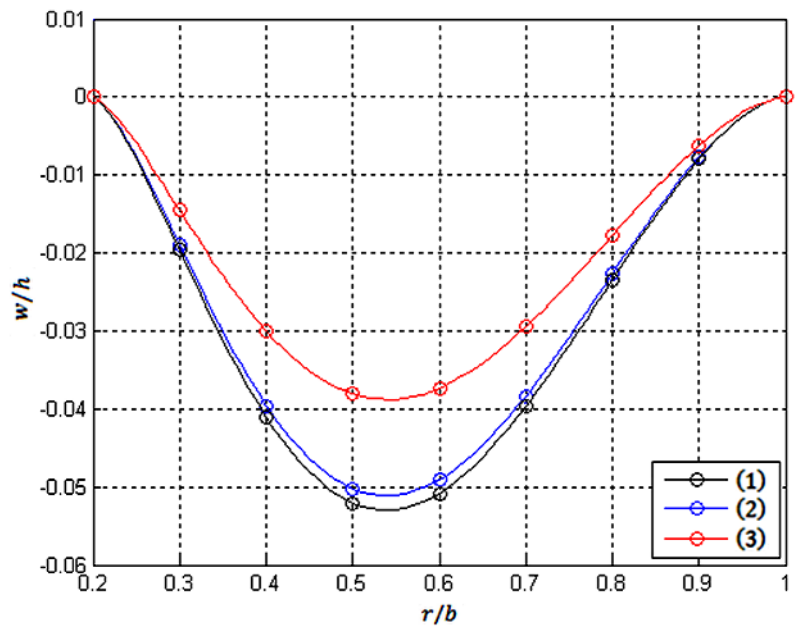
Figure 26   Influence of the foundation stiffness on the radial variations of the dimensionless lateral displacement of the bottom surface of the two-directional functionally graded clamped annular plate.
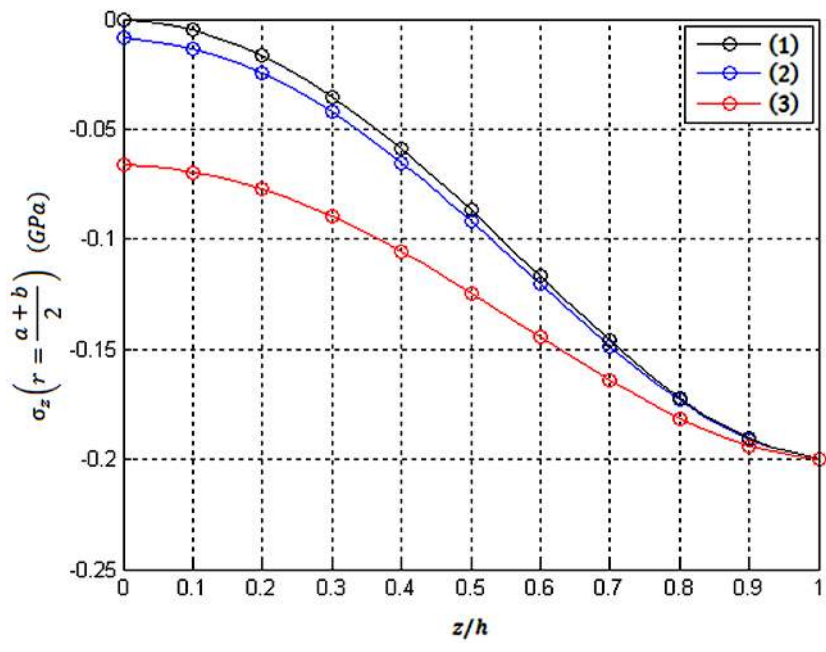

Figure 27   Influence of the foundation stiffness on the through-the-thickness distribution of the transverse normal stress of the two-directional functionally graded clamped annular plate.
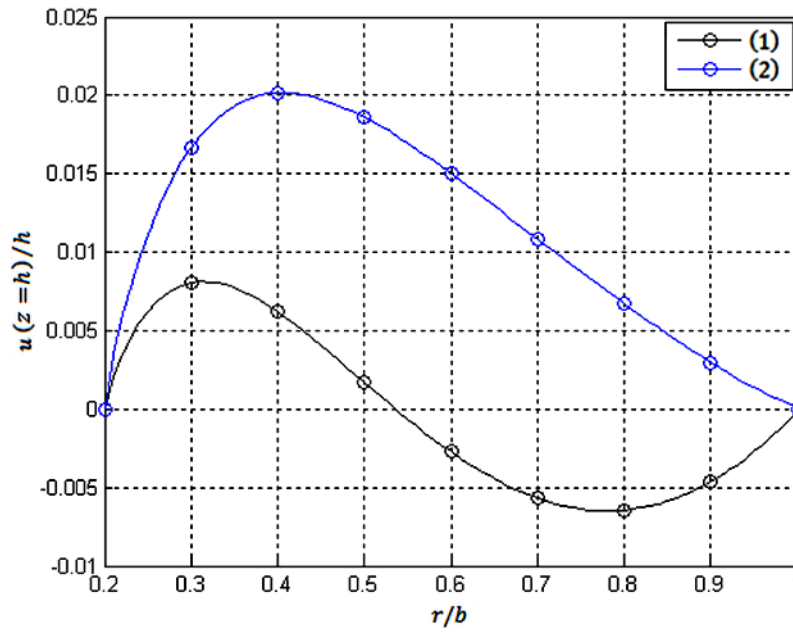
Figure 28   Effect of the angular speed on the dimensionless radial displacement component of the top surface of the transversely loaded two-directional functionally graded annular plate: (1) stationary plate, (2) rotating plate [analysis (iv)].

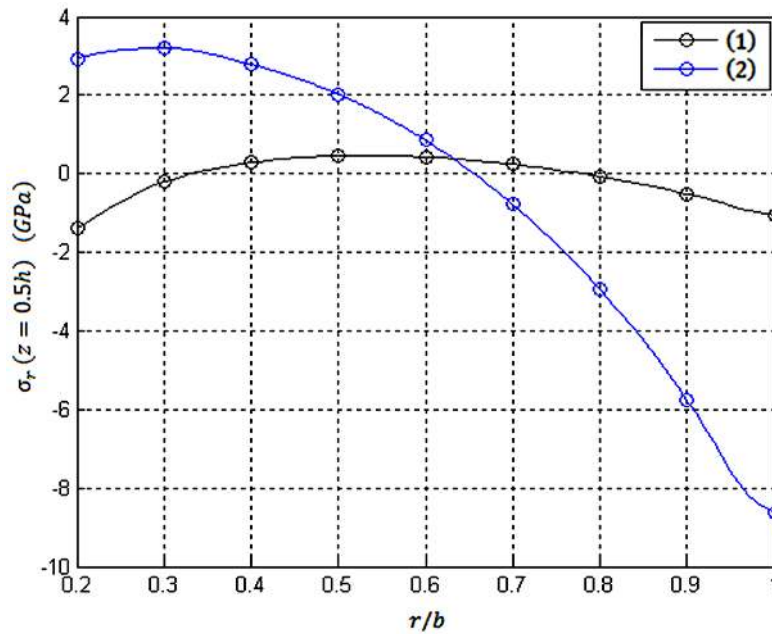
Figure 29   Effect of the angular speed on the radial stress of the mid-surface of the transversely loaded two-directional functionally graded annular plate: (1) stationary plate, (2) rotating plate [analysis (iv)].

5 CONCLUSIONS

In the present paper, a Hermitian finite element bending and stress analysis is presented for two-directional functionally graded circular/annular plates and disks for the first time, employing the three-dimensional theory of elasticity.

Some of the innovations incorporated in the present research are:

- Comprehensive analysis of the two-directional functionally graded annular and circular plates.
- Using the three-dimensional theory of elasticity, for various combinations of the loading and edge conditions. Mixed (Dirichlet-type and Neumann-type) boundary conditions may be applied based on the presented solution algorithm.
- Effects of the angular speed are considered in conjunction with the material heterogeneity. Therefore, the resulted bending-extensional coupling is implicitly taken into account.
- The plate may be supported by a non-uniform elastic foundation.
- The proposed formulation and the presented results are comprehensive and cover many practical applications.
- In contrast to the very limited works presented for the rotating functionally graded circular plates so far, the through-the-thickness stress distribution and bending of the loaded plates are investigated. Furthermore, the loads may vary in an arbitrary pattern in the radial direction.
- Some of the practical annular/circular plates considered in the results section are:
  a) Stationary annular/circular plates.
  b) Radially-graded, transversely-graded, and two-directional graded heterogeneous annular and circular plates and disks.
  c) Plates resting on soft or rigid substrates and plates without elastic foundations.
  d) Rotating plates with the specifications mentioned in items (b) and (c).

Results reveal that choosing a proper material distribution may lead to a more suitable stress distribution, enhance the sections rigidity or shift the critical points with respect to the displacement components. On the other hand, the angular speed may alter the nature of the stresses of the transversely loaded annular plate or disk.

References

Alipour, M.M., Shariyat, M., Shaban, M., (2010). A semi-analytical solution for free vibration of variable thickness two-directional-functionally graded plates on elastic foundations. International Journal of Mechanics and Materials in Design 6(4): 293-304.

Alipour, M.M., Shariyat, M., (2011). Semi-analytical buckling analysis of heterogeneous variable thickness viscoelastic circular plates on elastic foundations. Mechanics Research Communications 38: 594-601.

Bayat, M., Sahari, B.B., Saleem, M., Ali, A., Wong, S.V., (2009a). Bending analysis of a functionally graded rotating disk based on the first order shear deformation theory. Applied Mathematical Modelling 33: 4215–4230.

Bayat, M., Sahari, B.B., Saleem, M., Ali, A., Wong, S.V., (2009b). Thermoelastic solution of a functionally graded variable thickness rotating disk with bending based on the first-order shear deformation theory. Thin-Walled Structures 47: 568–582.

Chen, J.-Y., Chen, W.-Q., (2007). 3D analytical solution for a rotating transversely isotropic annular plate of functionally graded materials. Journal of Zhejiang University Science A 8(7): 1038-1043.

Chen, J.-Y., Ding, H.-J., Chen, W.-Q., (2007). Three-dimensional analytical solution for a rotating disc of functionally graded materials with transverse isotropy. Archive of Applied Mechanics 77: 241–251.

Garcia, O.A., Proença, S.P.B., (2007). Linear analysis of axis-symmetric plates and shells by the generalized Finite Element Method. Latin American Journal of Solids and Structures 4: 121-147.

Golmakani, M.E., Kadkhodayan, M., (2011). Nonlinear bending analysis of annular FGM plates using higher-order shear deformation plate theories. Composite Structures 93: 973–982.

Hosseini Kordkheili, S.A., Naghdabadi, R., (2007). Thermoelastic analysis of a functionally graded rotating disk. Composite Structures 79: 508–516.

Kim, W., Reddy, J.N., (2010). Novel mixed finite element models for nonlinear analysis of plates. Latin American Journal of Solids and Structures 7: 201–226.

Lei, Z., Zheng, Z., (2009). Exact solution for axisymmetric bending of functionally graded circular plate. Tsinghua Science and Technology 14: 64-68.

Li, X.Y., Ding, H.J., Chen, W.Q., (2008a). Elasticity solutions for a transversely isotropic functionally graded circular plate subject to an axisymmetric transverse load qr^k. International Journal of Solids and Structures 45: 191–210.

Li, X.Y., Ding, H.J., Chen, W.Q., (2008b). Three-dimensional analytical solution for functionally graded magneto–electro-elastic circular plates subjected to uniform load. Composite Structures 83: 381–390.

Ma, L.S., Wang, T.J., (2004). Relationships between axisymmetric bending and buckling solutions of FGM circular plates based on third-order plate theory and classical plate theory. International Journal of Solids and Structures 41: 85–101.

Nie, G., Zhong, Z., (2007).Axisymmetric bending of two-directional functionally graded circular and annular plates. Acta Mechanica Solida Sinica 20: 289-295.

Nie, G.J., Zhong, Z., (2010). Dynamic analysis of multi-directional functionally graded annular plates. Applied Mathematical Modeling 34(3): 608–616.

Peng, X.-L., Li, X.-F., (2010). Thermal stress in rotating functionally graded hollow circular disks. Composite Structures 92: 1896–1904.

Polat, C., (2010). An assessment of a co-rotational EAS brick element. Latin American Journal of Solids and Structures 7: 77–89.

Reddy, J.N., (2006). An introduction to the finite element method. 2nd Edition, New York: Wiley.

Reddy, J.N., Wang, C.M., Kitipornchai, S., (1999). Axisymmetric bending of functionally graded circular and annular plates. European Journal of Mechanics A/Solids 18: 185-199.

Shariyat, M., (2009a). A nonlinear Hermitian transfinite element method for transient behavior analysis of hollow functionally graded cylinders with temperature-dependent materials under thermo-mechanical loads. International Journal of Pressure Vessels and Piping 86: 280-289.

Shariyat, M., (2009b). A rapidly convergent nonlinear transfinite element procedure for transient thermoelastic analysis of temperature-dependent functionally graded cylinders. Journal of Solid Mechanics 1(4): 313-327.

Shariyat, M., (2010a). Non-linear dynamic thermo-mechanical buckling analysis of the imperfect sandwich plates based on a generalized three-dimensional high-order global-local plate theory. Composite Structures 92: 72-85.

Shariyat, M., (2010b). A generalized high-order global-local plate theory for nonlinear bending and buckling analyses of imperfect sandwich plates subjected to thermo-mechanical loads. Composite Structures 92: 130-143.

Shariyat, M., (2011a). A nonlinear double-superposition global-local theory for dynamic buckling of imperfect viscoelastic composite/sandwich plates: a hierarchical constitutive model. Composite Structures 93: 1890-1899.

Shariyat, M., (2011b). An accurate double superposition global-local theory for vibration and bending analyses of cylindrical composite and sandwich shells subjected to thermomechanical loads. Proceedings of the Institution of Mechanical Engineers, Part C: Journal of Mechanical Engineering Science 225: 1816-1832.

Shariyat, M., (2011c). Nonlinear thermomechanical dynamic buckling analysis of imperfect viscoelastic composite/sandwich shells by a double-superposition global-local theory and various constitutive models. Composite Structures 93: 2833-2843.

Shariyat, M., (2012). A general nonlinear global-local theory for bending and buckling analyses of imperfect cylindrical laminated and sandwich shells under thermomechanical loads. Meccanica 47; 301-319.

Shariyat, M., Alipour, M.M., (2011). Differential transform vibration and modal stress analyses of circular plates made of two-directional functionally graded materials resting on elastic foundations. Archive of Applied Mechanics 81: 1289-1306.

Shariyat, M., Eslami, M.R., (1996). Isoparametric finite-element thermoelastoplastic creep analysis of shells of revolution. International Journal of Pressure Vessels and Piping 68(3): 249-259.

Shariyat, M., Khaghani, M., Lavasani, S.M.H., (2010). Nonlinear thermoelasticity, vibration, and stress wave propagation analyses of thick FGM cylinders with temperature-dependent material properties. European Journal of Mechanics A/Solids, 29: 378-391.

Shariyat, M., Lavasani, S.M.H., Khaghani, M., (2010b). Nonlinear transient thermal stress and elastic wave propagation analyses of thick temperature-dependent FGM cylinders, using a second-order point-collocation method. Applied Mathematical Modelling 34: 898-918.

Shariyat, M., Nikkhah, M., Kazemi, R., (2011). Exact and numerical elastodynamic solutions for thick-walled functionally graded cylinders subjected to pressure shocks. International Journal of Pressure Vessels and Piping 88: 75-87.

Sburlati, R., Bardella, L., (2011). Three-dimensional elastic solutions for functionally graded circular plates. European Journal of Mechanics A/Solids, 30: 219–235.

Wang, Y., Xu, R.Q., Ding, H.J., (2010). Three-dimensional solution of axisymmetric bending of functionally graded circular plates. Composite Structures 92: 1683–1693.

Yang, B., Ding, H.J., Chen, W.Q., (2008). Elasticity solutions for a uniformly loaded annular plate of functionally graded materials. Structural Engineering Mechanics 30(4): 501–12.

Zienkiewicz, O.C., Taylor, R.L., (2005). The Finite Element Method: Its Basis and Fundamentals. 6$^{\text{th}}$ edition, Butterworth-Heinemann.